Direct Complex Envelope Sampling with Nonuniformly Interleaved Two-Channel ADCs

Bernard C. Levy, Mansoor S. Wahab and Anthony Van Selow

***Abstract*—A general and flexible technique is proposed for sampling the complex envelope of a bandpass signal by using a nonuniformly interleaved two-channel analog-to-digital converter (ADC). The signal is sampled directly without any demodulation operation, but the two sampling channels are not uniformly interleaved, since some timing skews are forbidden. The proposed complex envelope sampling scheme requires the implementation of two digital FIR filters and a discrete-time modulator. Computer simulations illustrating the performance of the proposed complex envelope sampling method method are presented.**

***Keywords*—bandpass sampling, direct sampling, software defined radio, time interleaved A/D converter**

I. Introduction

Due to their lower hardare complexity, direct bandpass sampling front ends have become attractive for software defined radio and radar applications. However, the implementation of flexible high-resolution bandpass sampling systems presents some challenges. First, if a single ADC is used, and B represents the occupied bandwidth of the signal of interest (which differs from its maximum frequency), alias-free reconstruction of the bandpass signal is not guaranteed for all sampling frequencies Ω_s above the Nyquist frequency $2B$ [1], [2], [3, Sec. 6.4]. In addition to being greater than $2B$, Ω_s needs to satisfy conditions which ensure that aliasing does not take place between the negative and positive frequencies of the bandpass signal to be sampled. The restrictions placed on Ω_s by these conditions depend on the location of the frequency band occupied by the bandpass signal. This creates a significant challenge for software defined radio receivers since different sampling frequencies need to be selected for signals in different bands, even if they have the same bandwidth. As early as 1953, Kohlenberg recognized that a simple way of overcoming this constraint consists of using second-order sampling, i.e. time-interleaved sampling, where two separate ADCs operating with a time skew sample the signal with frequency $\Omega_s' = \Omega_s/2$. In this case, except for certain forbidden values of the timing offset between the two ADCs, the bandpass signal can be reconstructed from the two time-interleaved sample sequences for all sampling frequencies Ω_s above $2B$.

Whereas [1], [4], [5] focus on the reconstruction of the bandpass signal itself from its samples, for modulated signal, it is usually of greater interest to obtain the sampled in-phase and quadrature (I and Q) signal components, i.e., the sampled complex envelope of the signal. Following an observation of Grace and Pitt [6], Brown [7] proposed quadrature sampling where the two interleaved sub-ADCs have a time skew equal to a quarter of the carrier period, plus possibly an integer multiple of the carrier period. However, this sampling technique requires also that the carrier frequency should be an integer multiple of the sub-ADC sampling frequency, which makes it inconvenient for software radio applications. Other choices of the sampling frequency, carrier frequency, and sub-ADC offset were explored by Sun and Signell [8], [9], but they involve again constraints that make it difficult to design flexible receivers.

In this paper we consider the computation of the sampled complex envelope of a bandpass signal from the sequences produced by a two-channel time-interleaved ADC (TIADC) with timing offset dT_s', where $0 < d < 1$ and $T_s' = 2\pi/\Omega_s'$ denotes the sub-ADC sampling period. No assumption is made about the carrier frequency Ω_c, signal bandwidth B, sampling frequency Ω_s and timing offset d, except that the sampling frequency Ω_s should be above $2B$ and the carrier frequency $\Omega_c > B/2$, which ensures that the signal considered is a bandpass signal. It is shown that the evaluation of the sampled complex envelope requires the implementation of two FIR real filters. As mentioned earlier, certain timing offsets are forbidden, and precise a characterization of the forbidden offsets is provided in terms of an integer index specifying in which image band of the baseband the carrier frequency Ω_c is located.

The paper is organized as follows. A model expressing the two-channel time-interleaved ADC sampling sequences in terms of the corresponding sampled complex envelope sequence is described in Section II. This model is used in Section III to compute the sampled complex envelope by using two digital FIR filters and a digital modulator. Simulations are presented in Section IV which show the effectiveness of the proposed technique. Finally, conclusions and directions for further research are presented in Section V.

II. Complex envelope sampling model

Consider the bandpass signal

$$\begin{aligned} x_c(t) &= a_c(t)\cos(\Omega_c t) - b_c(t)\sin(\Omega_c t) \\ &= \Re[c_c(t)e^{j\Omega_c t}] = |c_c(t)|\cos(\Omega_c t + \angle c_c(t)) \,, \end{aligned} \quad (1)$$

where

$$c_c(t) = a_c(t) + jb_c(t) \quad (2)$$

This work was supported by NSF Grant ECCS-1444086.

Bernard C. Levy and and Anthony Van Selow are with the Department of Electrical and Computer Engineering, 1 Shields Avenue, University of California, Davis, CA 95616 (emails: bclevy, apvanselow@ucdavis.edu). After receiving a BS at UC Davis, Mansoor Wahab is now a graduate student in the Department of Electrical and Computer Engineering at Cornell University, Ithaca, NY 14853 (email: sw798@cornell.edu).

denotes the complex envelope of $x_c(t)$ and the in-phase and quadrature components $a_c(t)$ and $b_c(t)$ are baseband signals with bandwidth $B/2$. If the carrier frequency $\Omega_c > B/2$ (it is in general much larger), the Fourier spectrum $X_c(j\Omega)$ of $x_c(t)$ is contained in two disjoint positive and negative frequency bands $[\Omega_L, \Omega_H]$ and $[-\Omega_H, -\Omega_L]$ with $\Omega_L = \Omega_c - B/2$ and $\Omega_H = \Omega_c + B/2$, so that the occupied bandwidth of $x_c(t)$ is $\Omega_H - \Omega_L = B$. Unlike conventional heterodyne radar or communications receivers [10] which convert $x_c(t)$ to a lower IF frequency, and correlate it with two quadrature IF oscillators to obtain the sampled in-phase and quadrature components, we consider here a direct bandpass sampling receiver where two time-interleaved ADCs sample $x_c(t)$ as shown in Fig. 1.

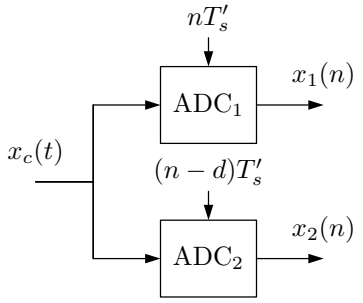

Fig. 1. Time-interleaved sampling of bandpass signal $x_c(t)$.

T_s' denotes the sampling period of the sub-ADCs, which have therefore sampling frequency $\Omega_s' = 2\pi/T_s' = \Omega_s/2$, where Ω_s denotes the sampling frequency of the overall ADC. It is assumed that $\Omega_s > 2B$, or equivalently $\Omega_s' > B$. The timing offset between the two ADCs is $D = dT_s'$ with $0 < d < 1$. For $d = 1/2$, the combination of the two sub-ADCs forms a uniform ADC with sampling period $T_s = T_s'/2$, but for $d \neq 1/2$, the overall ADC has a nonuniform but periodic sampling pattern. Note also that the use of a timing offset $d \neq 1/2$ implies that that the sub-ADCs cannot share the same S/H.

Let

$$\ell = \text{round}\Big(\frac{\Omega_c}{\Omega_s'}\Big)\,, \tag{3}$$

so that Ω_c belongs to the frequency band $[(\ell - 1/2)\Omega_s', (\ell + 1/2)\Omega_s']$. Since this frequency band corresponds to the location of the ℓ-th image copy of a sampled baseband signal, it is referred to here as the ℓ-th image band. In the following it is assumed that $\ell \geq 1$, so that the signal $x_c(t)$ is a bandpass signal. Since the band $[(\ell - 1/2)\Omega_s', (\ell + 1/2)\Omega_s']$ includes the 2ℓ-th and $2\ell + 1$-th Nyquist zones of the sub-ADCs, ℓ can be expressed in terms the Nyquist zone index k as $\ell = \lfloor k/2 \rfloor$. If we consider the discrete modulation frequency

$$\omega_b = \Omega_c T_s' \bmod 2\pi = \Big(\frac{\Omega_c}{\Omega_s'} - \ell\Big)2\pi\,, \tag{4}$$

so that $-\pi < \omega_b \leq \pi$, the sampled sequence $x_1(n)$ can be expressed as

$$x_1(n) = x_c(nT_s') = \Re\{c(n)e^{j\omega_b n}\} \tag{5}$$

where $c(n) = c_c(nT_s')$ denotes the sampled complex envelope. Similarly by observing that

$$e^{j(n-d)\Omega_c T_s'} = e^{j(n-d)(\omega_b + 2\pi\ell)} = e^{j\omega_b(n-d)}e^{-j2\pi\ell d}$$

we can express the sampled sequence $x_2(n)$ as

$$x_2(n) = x_c((n-d)T_s') = \Re\{c(n-d)e^{j\omega_b(n-d)}e^{-j2\pi\ell d}\}. \tag{6}$$

In this expression $c(n-d)$ is a shorthand notation for

$$c(n-d) = f(n) * c(n) \tag{7}$$

where $*$ represents the discrete convolution operation and

$$f(n) = \frac{\sin(\pi(n-d))}{\pi(n-d)} \tag{8}$$

is the impulse response of the periodic fractional delay filter specified by

$$F(e^{j\omega}) = e^{-j\omega d}$$

for $-\pi < \omega \leq \pi$. More generally, the 2π periodic filter $F(e^{j\omega})$ can be expressed as

$$F(e^{j\omega}) = e^{-j(\omega - q(\omega))d} \tag{9}$$

for all ω, where

$$q(\omega) = k2\pi \quad \text{for} \quad (2k-1)\pi \leq \omega < (2k+1)\pi$$

represents the quantized value of ω produced by an infinite quantizer with step size 2π.

The Fourier transform of sequence

$$s(n) = c(n-d)e^{j\omega_b(n-d)}e^{-j2\pi\ell d} \tag{10}$$

appearing in (6) is given by

$$\begin{aligned} S(e^{j\omega}) &= F(e^{j(\omega-\omega_b)})C(e^{j(\omega-\omega_b)})e^{-j(\omega_b+2\pi\ell)d} \\ &= F(e^{j\omega})G(e^{j\omega})C(e^{j(\omega-\omega_b)})\,, \end{aligned} \tag{11}$$

where

$$C(e^{j\omega}) = \sum_{n=-\infty}^{\infty} c(n)e^{-j\omega n} \tag{12}$$

denotes the discrete-time Fourier transform (DTFT) of $c(n)$ and the filter

$$\begin{aligned} G(e^{j\omega}) &\triangleq \frac{F(e^{j(\omega-\omega_b)})}{F(e^{j\omega})}e^{-j(\omega_b+2\pi\ell)d} \\ &= e^{-j(q(\omega)-q(\omega-\omega_b))d}e^{-j2\pi\ell d} \end{aligned} \tag{13}$$

is a piecewise constant frequency dependent phase shift. For $\omega_b > 0$, it can be expressed as

$$G(e^{j\omega}) = \begin{cases} e^{-j2\pi(\ell+1)d} & -\pi \leq \omega < -\pi + \omega_b \\ e^{-j2\pi\ell d} & -\pi + \omega_b \leq \omega < \pi\,, \end{cases} \tag{14}$$

and for $\omega_b < 0$, we have

$$G(e^{j\omega}) = \begin{cases} e^{-j2\pi\ell d} & -\pi \leq \omega \leq \pi + \omega_b \\ e^{-j2\pi(\ell-1)d} & \pi + \omega_b < \omega < \pi\,. \end{cases} \tag{15}$$

Since the impulse response $f(n)$ of fractional delay filter $F(e^{j\omega})$ is real, the discrete-time model (5)–(6) can be represented in block diagram form as shown in Fig. 2. In this model,

$F(e^{j\omega})$ describes the relative timing skew between the two sub-ADCs, whereas the filter $G(e^{j\omega})$ depends on the image band index ℓ of Ω_c and its relative location ω_b within this band. Thus, from a software defined radio perspective, $G(e^{j\omega})$ changes if the frequency band of the signal of interest varies, but $F(e^{j\omega})$ stays the same.

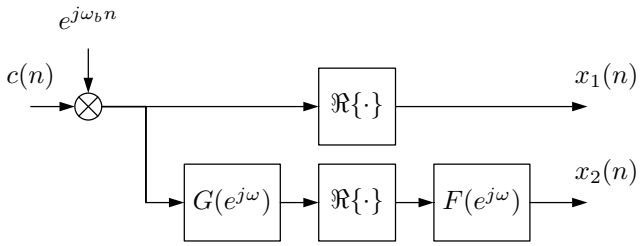

Fig. 2. Discrete-time bandpass sampling model

III. Complex envelope computation

We consider the problem of recovering $c(n)$ from $x_1(n)$ and $x_2(n)$. Note first that since $c(n)$ is complex, $C(e^{j\omega})$ is devoid of symmetries, so knowledge of $C(e^{j\omega})$ over the entire frequency band $[-\pi, \pi]$ is needed to recover $c(n)$. The DTFTs of $x_1(n)$ and $x_2(n)$ are given by

$$X_1(e^{j\omega}) = \frac{1}{2}[C(e^{j(\omega-\omega_b)}) + C^*(e^{-j(\omega+\omega_b)})] \quad (16)$$

and

$$\begin{aligned} X_2(e^{j\omega}) &= \frac{F(e^{j\omega})}{2}[G(e^{j\omega})C(e^{j(\omega-\omega_b)}) \\ &\quad +G^*(e^{-j\omega})C^*(e^{-j(\omega+\omega_b)})]\,. \end{aligned} \quad (17)$$

In each of these expressions, the superposition of $C(e^{j(\omega-\omega_b)})$ and $C^*(e^{-j(\omega+\omega_b)})$ makes it impossible to recover each of these functions separately from either $X_1(e^{j\omega})$ or $X_2(e^{j\omega})$ alone. But (16) and (17) can be written together in matrix form as

$$\begin{bmatrix} X_1(e^{j\omega}) \\ F^{-1}(e^{j\omega})X_2(e^{j\omega}) \end{bmatrix} = \mathbf{M}(e^{j\omega}) \begin{bmatrix} C(e^{j(\omega-\omega_b)}) \\ C^*(e^{-j(\omega+\omega_b)}) \end{bmatrix}, \quad (18)$$

where the matrix

$$\mathbf{M}(e^{j\omega}) = \frac{1}{2}\begin{bmatrix} 1 & 1 \\ G(e^{j\omega}) & G^*(e^{-j\omega}) \end{bmatrix} \quad (19)$$

is invertible as long as its determinant

$$D(e^{j\omega}) = \frac{1}{4}(G^*(e^{-j\omega}) - G(e^{j\omega}) \quad (20)$$

is nonzero. We find

$$D(e^{j\omega}) = \frac{j}{2}\sin(2\pi\ell d)$$

for $0 \le |\omega| \le \pi - |\omega_b|$, and

$$D(e^{j\omega}) = \frac{j}{2}e^{j\pi\mathrm{sgn}(\omega)d}\sin(\pi(2\ell + \mathrm{sgn}(\omega_b))d)$$

for $\pi - |\omega_b| < |\omega| < \pi$, where $\mathrm{sgn}(\omega)$ denotes the sign of ω. Accordingly, the determinant $D(e^{j\omega})$ will be nonzero as long as the timing skew d is such that both $\sin(2\pi\ell d)$ and $\sin(\pi(2\ell + \mathrm{sgn}(\omega_b)))$ are nonzero. The values

$$d_m^i = \frac{m}{2\ell} \quad (21)$$

with m integer such that $0 \le m \le 2\ell - 1$, and

$$d_m^e = \frac{q}{2\ell + \mathrm{sgn}(\omega_b)} \quad (22)$$

with q integer such that $1 \le q \le 2\ell + \mathrm{sgn}(\omega_b) - 1$, form the *forbidden timing offsets*. Note that for $m = \ell$, we have $d_\ell^i = 1/2$, so as expected, the half sampling period is a forbidden offset, since in this case the TIADC reduces to a uniform ADC with sampling period $T_s = T_s'/2$.

When $\mathbf{M}(e^{j\omega})$ is invertible for all ω, we obtain

$$C(e^{j(\omega-\omega_b)}) = H_1(e^{j\omega})X_1(e^{j\omega}) + H_2(e^{j\omega})X_2(e^{j\omega}) \quad (23)$$

where the filters

$$\begin{aligned} &\begin{bmatrix} H_1(e^{j\omega}) & H_2(e^{j\omega}) \end{bmatrix} \\ &= \begin{bmatrix} 1 & 0 \end{bmatrix}\mathbf{M}^{-1}(e^{j\omega})\begin{bmatrix} 1 & 0 \\ 0 & F^{-1}(e^{j\omega}) \end{bmatrix} \\ &= \frac{1}{2D(e^{j\omega})}\begin{bmatrix} G^*(e^{-j\omega}) & -F^{-1}(e^{j\omega}) \end{bmatrix}. \end{aligned} \quad (24)$$

Since $C(e^{j(\omega-\omega_b)})$ is the Fourier transform of the modulated signal $r(n) = e^{j\omega_b n}c(n)$, $c(n)$ can be recovered by demodulating $r(n)$, as shown in Fig. 3.

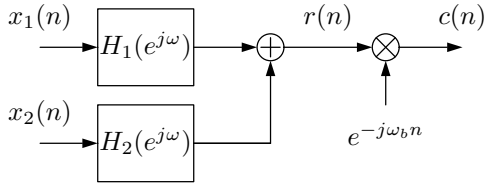

Fig. 3. Recovery of $c(n)$ from $x_1(n)$ and $x_2(n)$

Substituting the expressions for $D(e^{j\omega})$ and $G(e^{j\omega})$ inside (24) gives

$$H_1(e^{j\omega}) = \frac{e^{j2\pi\ell d}}{j\sin(2\pi\ell d)} = 1 - j\cot(2\pi\ell d) \quad (25)$$

for $|\omega| \le \pi - |\omega_b|$ and

$$\begin{aligned} H_1(e^{j\omega}) &= \frac{e^{j\pi(2\ell+\mathrm{sgn}(\omega_b))d}}{j\sin(\pi(2\ell+\mathrm{sgn}(\omega_b))d)} \\ &= 1 - j\cot(\pi(2\ell+\mathrm{sgn}(\omega_b))d) \end{aligned} \quad (26)$$

for $\pi - |\omega_b| < |\omega| \le \pi$. Similarly, we find

$$H_2(e^{j\omega}) = j\frac{e^{j\omega d}}{\sin(2\pi\ell d)} \quad (27)$$

for $|\omega| \le \pi - |\omega_b|$ and

$$H_2(e^{j\omega}) = j\frac{e^{j(\omega-\pi\mathrm{sgn}(\omega))d}}{\sin(\pi(2\ell+\mathrm{sgn}(\omega_b))d)} \quad (28)$$

for $\pi - |\omega_b| < |\omega| < \pi$. The impulse responses of filters H_1 and H_2 can be evaluated in closed form and are given by

$$\Re\{h_1(n)\} = \delta(n) \quad , \quad \Re\{h_2(n)\} = 0 \tag{29}$$

$$\begin{aligned}\Im\{h_1(n)\} = &-\cot(\pi(2\ell+\mathrm{sgn}(\omega_b))d)\delta(n)\\ &+\big(\cot(\pi(2\ell+\mathrm{sgn}(\omega_b))d) - \cot(2\pi\ell d)\big)\\ &\times\frac{\sin((\pi-|\omega_b|)n)}{\pi n}\,,\end{aligned} \tag{30}$$

and

$$\begin{aligned}\Im\{h_2(n)\} &= \frac{\sin((\pi-|\omega_b|)(n+d))}{\pi\sin(2\pi\ell d)(n+d)}\\ &\quad -\frac{\sin((\pi-|\omega_b|)(n+d)-\pi d)}{\pi\sin(\pi(2\ell+\mathrm{sgn}(\omega_b)d)(n+d)}\,.\end{aligned} \tag{31}$$

The IIR impulse responses $h_1(n)$ and $h_2(n)$ can be approximated by causal filters of order $M = 2L$ by shifting the impulse responses by L and applying a Kaiser window of order $M+1$. In this case, the output $\hat{c}(n-L)$ of the reconstruction block diagram is only an estimate of the complex envelope at time $n-L$. Since the sequences $x_1(n)$ and $x_2(n)$ are real, and each of the complex filters H_1 and H_2 requires only the implementation of a single real FIR filter, the complexity of the reconstruction technique depicted in Fig. 3 is $2(M+1)$ real multiplications and one complex multiplication per complex envelope sample (the complex multiplication is needed to implement the $e^{-j\omega_b(n-L)}$ discrete-time demodulation).

It is also worth pointing put that unlike previously published results on TIADC sampling of the envelope of bandpass signals, no restriction is placed here on Ω_c, Ω_s, B and d beyond $\Omega_c > \Omega_s/2 > B$ (Ω_c cannot be in the baseband and Ω_s is above the Nyquist rate). Earlier results [7]–[9] typically assume relations between Ω_s and Ω_c and between d and Ω_c. For example for quadrature sampling [7], [11], $\Omega_s' = \Omega_c/\ell$ with ℓ integer, so that Ω_c is exactly at the center of the ℓ-th image band, and $D = T_c/4 + qT_c$ with q integer. In this case $\omega_b = 0$ and

$$d = \frac{D}{T_s'} = \frac{1}{4\ell} + \frac{q}{\ell}$$

so $2\pi\ell d = \pi/2 + 2\pi q$. In this case equations (5) and (6) reduce to

$$\begin{aligned}x_1(n) &= a(n) = a_c(nT_s')\\ x_2(n) &= b(n-d) = b_c((n-d)T_s')\,,\end{aligned}$$

so that the two sub-ADCs sample independently the in-phase and quadrature components of the bandpass signal. In spite of the elegance of this solution, the presence of clock jitter makes it nearly impossible to ensure that Ω_s' is precisely an integer fraction of Ω_c. In this respect, it is useful to keep in mind that a desirable attribute of software defined radio or radar receivers is their potential ability to operate in many different frequency bands. By this metric, the proposed envelope sampling scheme is rather flexible, since a change in carrier frequency Ω_c requires only a recomputation of the digital filters H_i, $i = 1, 2$ which depend on the image band index ℓ of Ω_c and digital frequency ω_b

IV. Simulations

To illustrate the proposed direct complex envelope sampling method, consider a bandpass signal with $F_c = \Omega_c/(2\pi) = 5.15$GHz, and continuous-time envelope

$$\begin{aligned}c_c(t) &= 2\cos(400\times10^6\times2\pi t)\\ &\quad +j[\sin(400\times10^6\times2\pi t)+\cos(175\times10^6\times2\pi t)]\\ &= \frac{3}{2}e^{j400\times10^6\times2\pi t}+\frac{1}{2}e^{-j400\times10^6\times2\pi t}\\ &\quad +\frac{j}{2}[e^{j175\times10^6\times2\pi t}+e^{-j175\times10^6\times2\pi t}]\end{aligned} \tag{32}$$

with bandwidth $B/(4\pi) = 400$MHz. The sub-ADC sampling frequency $F_s' = \Omega_s'/(2\pi) = 1$GHz is above $B/(2\pi) = 800$MHz, as required by the Nyquist sampling criterion. Since

$$F_c = 5F_s' + 150\,,$$

we have $\ell = 5$, i.e., F_c is located in the 5-th image band, and

$$\omega_b = \frac{150}{1000}\times 2\pi = 0.3\pi\,.$$

The discrete-time envelope obtained by sampling $c_c(t)$ with sampling period $T_s' = 1/F_s'$ is

$$\begin{aligned}c(n) = c_c(nT_s') &= \frac{3}{2}e^{j0.8\pi n}+\frac{1}{2}e^{-j0.8\pi n}\\ &\quad +\frac{j}{2}[e^{j0.35\pi n}+e^{-j0.35\pi n}]\end{aligned} \tag{33}$$

This signal has four tones located at $\pm0.8\pi$ and $\pm0.35\pi$, but the tone at 0.8π has an amplitude three times larger than the tones at -0.8π and $\pm0.35\pi$.

To sample $x_c(t)$, we select a TIADC with timing offset $d = 0.425$, which is approximately half-way between two forbidden timing offsets: $d_4^i = 0.4$ and $d_5^e = 0.454$. In the simulations two independent white noise sequences modelling the effect of thermal and quantization noises are added to the sub-ADC outputs. The sub-ADC SNR is 61.8dB. The filters $H_i(z)$ with $i = 1, 2$ of Fig. 3 have order $M = 60$ and are obtained by applying a Kaiser window with parameter $\beta = 6$ to the IIR impulse responses $h_1(n)$ and $h_2(n)$ given in (29)–(31).

The power spectral density (PSD) of the estimated envelope is shown in Fig. 4. It is evaluated by using the windowed complex data periodogram method for a data block of length $N = 10^4$ samples. The periodogram is scaled so that a complex tone with unit amplitude corresponds to 0dB. In addition to the four desired tones at $\pm0.8\pi$ and $\pm0.35\pi$, four secondary tones are present representing the residual spectral components of $e^{-j2\omega_b n}c^*(n) = e^{-j0.6\pi n}c^*(n)$, which are located at 0.6π, 0.2π, -0.25π, and -0.95π. Since the dominant tone of $c^*(n)$ is located at -0.8π, the highest secondary tone in the PSD of $\hat{c}(n)$ is located at $0.6\pi = -0.6\pi - 0.8\pi \mod(2\pi)$, yielding a SFDR of about 65dB. It is worth also noting that the secondary tone at -0.95π is higher than the secondary tones at -0.25π and 0.2π which should in theory have the same level. This is due to the fact that the filters $H_1(e^{j\omega})$ and $H_2(e^{j\omega})$ have discontinuities at $\pm(1-|\omega_b|)\pi = \pm0.7\pi$ so that after windowing, the filters exhibit nonideal filtering characteristics in transition bands about these discontinuity points. After

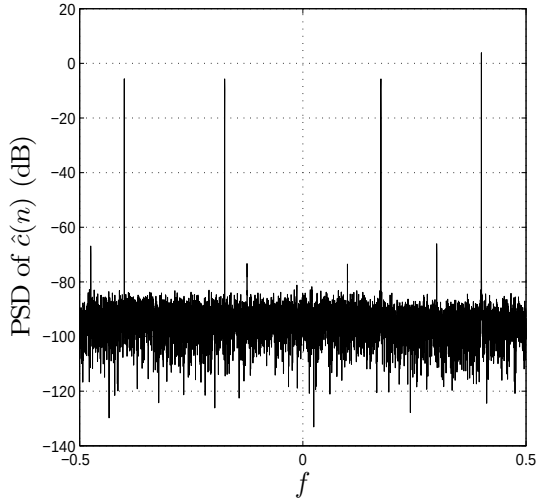

Fig. 4. PSD of the estimated envelope $\hat{c}(n)$ computed with FIR filters of order 60 for a TIADC with timing skew $d = 0.425$.

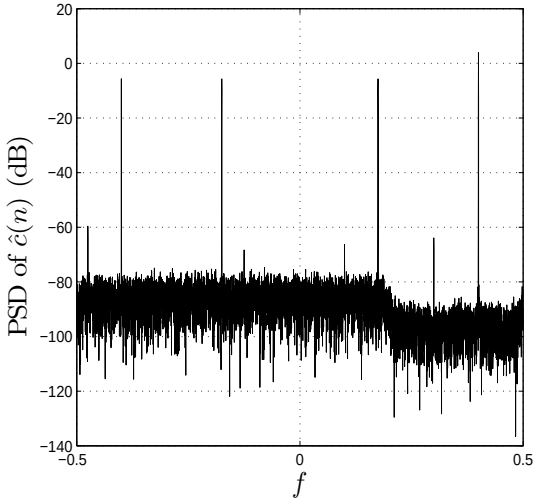

Fig. 5. PSD of the estimated envelope $\hat{c}(n)$ computed with FIR filters of order 60 for a TIADC with $d = 0.401$.

modulation by $e^{-j\omega_b n} = e^{-j0.3\pi n}$, the nonideal filtering bands become located about $-\pi$ and 0.4π, which explains the higher level of the secondary tone at -0.95π. Finally, since the exact envelope $c(n)$ is known, the error $\tilde{c}(n) = c(n) - \hat{c}(n)$ can be evaluated, and the mean-square error (MSE) is -53.54dB.

To illustrate the slight degradation in performance which occurs if the timing skew d is close to a forbidden value, consider the case where $d = d_4^i + 0.001 = 0.401$ is close to forbidden value d_4^i. The PSD of the computed sampled complex envelope of signal $x_c(t)$ is shown in Fig. 5. The secondary tones are approximately at the same level as in Fig. 4, but the a piecewise constant filtering operation is applied the the noise floor. This is due to the fact that since $D(e^{j\omega})$ is close to zero inside interval $[-0.7\pi, 0.7\pi]$ the magnitudes of filters $H_i(e^{j\omega})$ with $i = 1, 2$ are not evaluated as accurately inside this band as outside. After demodulation by $e^{-0.3\pi n}$, the effect of mismatched filter magnitudes is exhibited in bands $[-\pi, 0.4\pi]$ and $[0.4\pi, \pi]$. The MSE becomes -47.27dB, so that a bad timing skew positioning results in a slight performance loss.

V. Conclusions

In this paper we have described a technique for computing the sampled complex envelope of a bandpass signal by sampling the signal directly with a two-channel TIADC. The proposed sampling technique has the potential to simplify greatly RF communications and radar receiver front-ends by removing all mixing and filtering hardware typically used to extract the I and Q components of the received signal prior to sampling. As was noted in [1], [4], the use of a non-uniform TIADC has also the advantage that sampling a bandpass signal of bandwidth B at rates slightly above $2B$ becomes possible, independently of the frequency band $[\Omega_L, \Omega_H]$ where the signal is located. Thus the proposed TIADC and reconstruction filter architecture could be implemented as a software radio front end capable of digitizing signals in different bands. The analysis presented here ignores the effect of TIADC mismatches. A blind calibration technique to estimate and correct timing and gain mismatches is presented in [12].

References

[1] A. Kohlenberg, "Exact interpolation of band-limited functions," *J. Applied Physics*, vol. 24, pp. 1432–1436, Dec. 1953.

[2] R. G. Vaughan, N. L. Scott, and D. R. White, "The theory of bandpass sampling," *IEEE Trans. Sig. Proc.*, vol. 39, pp. 1973–1984, Sept. 1991.

[3] J. G. Proakis and D. G. Manolakis, *Digital Signal Processing: Principles, Algorithms, and Applications, 4th edition*. Upper Saddle River, NJ: Prentice-Hall, 2007.

[4] A. J. Coulson, "A generalization of nonuniform bandpass sampling," *IEEE Trans. Sig. Proc.*, vol. 41, pp. 694–704, Mar. 1995.

[5] Y.-P. Lin and P. P. Vaidyanathan, "Periodically nonuniform sampling of bandpass signals," *IEEE Trans. Sig. Proc.*, vol. 45, pp. 340–351, Mar. 1998.

[6] O. D. Grace and S. P. Pitt, "Quadrature sampling of high frequency waveforms," *J. Acoust. Soc. Amer.*, vol. 44, pp. 1453–1454, 1968.

[7] J. L. Brown, Jr., "On quadrature sampling of bandpass signals," *IEEE Trans. Aerospace Elec. Syst.*, vol. 15, May 1979.

[8] Y.-R. Sun and S. Signell, "Generalized bandpass sampling with FIR filtering," in *Proc. 2005 IEEE Internat. Symp. Circuits Systems*, (Kobe, Japan), pp. 4429–4432, May 2005.

[9] Y.-R. Sun, *Generalized bandpass sampling receivers of software defined radio*. PhD thesis, Royal Institute of Technology, Stockholm, Sweden, 2006.

[10] S. Mirabassi and K. Martin, "Classical and modern receiver architectures," *IEEE Communic. Magazine*, Nov. 2000.

[11] A. G. Dempster, "Quadrature bandpass sampling rules for single- and multiband communications and satellite navigation receivers," *IEEE Trans. Aerospace Elec. Syst.*, vol. 47, Oct. 2011.

[12] B. C. Levy, A. Van Selow, and M. Wahab, "Blind calibration of a nonuniformly interleaved bandpass sampling two-channel ADC." Submitted for publication to IEEE TCAS I.